Research Article | Vol. 25, No. 26 | 25 Dec 2017 | OPTICS EXPRESS 33504
Optics EXPRESS

All-optical digital-to-spike conversion using a graphene excitable laser

PHILIP Y. MA,* BHAVIN J. SHASTRI, THOMAS FERREIRA DE LIMA, ALEXANDER N. TAIT, MITCHELL A. NAHMIAS, AND PAUL R. PRUCNAL

Department of Electrical Engineering, Princeton University, Princeton, NJ 08544, USA
*yechim@princeton.edu

Abstract: Neuromorphic (brain-inspired) photonic systems process information encoded in the pulses of light, i.e., "spikes" that are analog in time but digital in amplitude. Applying these systems to process commonly used digital data requires a simple and effective interfacing solution to converting binary digits into spike sequence in the optical domain. Laser systems offer a variety of useful nonlinear functionalities, including excitable dynamics that can be found in the time-resolved "spiking" of neurons. We propose and demonstrate, both numerically and experimentally, an all-optical digital-to-spike (DTS) conversion scheme using a single graphene excitable laser (GEL) without clock signal synchronization. We first study the DTS conversion mechanism based on the simulation platform of an integrated GEL, which achieve a DTS conversion rate up to 10 Gbps. Our DTS conversion scheme can be operated under flexible input power conditions and exhibits a strong logic-level restoration capability. We then verify the feasibility of our approach via a proof-of-principle experiment where a fiber-based GEL obtains a DTS conversion rate of 40 Kbps, and a bit error rate (BER) of 10^{-9} with an input power of −24 dBm. This technology can be potentially applied in future neuromorphic photonic systems for information processing and computing.

OCIS codes: (070.4340) Nonlinear optical signal processing; (230.1150) All-optical devices; (320.7085) Ultrafast information processing.

References and links

1. R. Sarpeshkar, "Analog versus digital: extrapolating from electronics to neurobiology," Neural Comput. **10**, 1601–1638 (1998).
2. A. Borst and F. E. Theunissen, "Information theory and neural coding," Nat. Neurosci. **2**, 947–957 (1999).
3. A. Kumar, S. Rotter, and A. Aertsen, "Spiking activity propagation in neuronal networks: reconciling different perspectives on neural coding," Nat Rev Neurosci. **11**, 615–627 (2010).
4. J. Schemmel, D. Briiderle, A. Griibl, M. Hock, K. Meier, and S. Millner, "A wafer-scale neuromorphic hardware system for large-scale neural modeling," in Proceedings of 2010 IEEE International Symposium on Circuits and Systems, (IEEE, 2010), pp. 1947–1950.
5. S. Furber, F. Galluppi, S. Temple, and L. Plana, "The spinnaker project," Proceedings of the IEEE **102**, 652–665 (2014).
6. B. V. Benjamin, P. Gao, E. McQuinn, S. Choudhary, A. R. Chandrasekaran, J. M. Bussat, R. Alvarez-Icaza, J. V. Arthur, P. A. Merolla, K. Boahen, "Neurogrid: A mixed-analog-digital multichip system for large-scale neural simulations," Proceedings of the IEEE **102**, 699–716 (2014).
7. P. A. Merolla, J. V. Arthur, R. Alvarez-Icaza, A. S. Cassidy, J. Sawada, F. Akopyan, B. L. Jackson, N. Imam, C. Guo, Y. Nakamura, B. Brezzo, I. Vo, S. K. Esser, R. Appuswamy, B. Taba, A. Amir, M. D. Flickner, W. P. Risk, R. Manohar, and D. S. Modha, "A million spiking-neuron integrated circuit with a scalable communication network and interface," Science **345**, 668–673 (2014).
8. M. A. Nahmias, B. J. Shastri, A. N. Tait, and P. R. Prucnal, "A leaky integrate-and-fire laser neuron for ultrafast cognitive computing," IEEE J. Sel. Topics. Quantum Electron. **19**, 1800212 (2013).
9. L. Gelens, L. Mashal, S. Beri, W. Coomans, G. Van der Sande, J. Danckaert, and G. Verschaffelt, "Excitability in semiconductor microring lasers: Experimental and theoretical pulse characterization," Phys. Rev. A **82**, 063841 (2010).
10. K. Alexander, T. Van Vaerenbergh, M. Fiers, P. Mechet, J. Dambre, and P. Bienstman, "Excitability in optically injected microdisk lasers with phase controlled excitatory and inhibitory response," Opt. Express **21**, 26182 (2013).

#309077 https://doi.org/10.1364/OE.25.033504
Journal © 2017 Received 13 Oct 2017; revised 7 Dec 2017; accepted 9 Dec 2017; published 22 Dec 2017

Optics EXPRESS

11. B. Romeira, J. Javaloyes, C. N. Ironside, J. M. L. Figueiredo, S. Balle, and O. Piro, "Excitability and optical pulse generation in semiconductor lasers driven by resonant tunneling diode photo-detectors," Opt. Express **21**, 20931–20940 (2013).
12. A. Aragoneses, S. Perrone, T. Sorrentino, M. C. Torrent, and C. Masoller, "Unveiling the complex organization of recurrent patterns in spiking dynamical systems," Sci. Rep. **4**, 4696 (2014).
13. F. Selmi, R. Braive, G. Beaudoin, I. Sagnes, R. Kuszelewicz, and S. Barbay, "Relative refractory period in an excitable semiconductor laser," Phys. Rev. Lett. **112**, 183902 (2014).
14. A. Hurtado, and J. Javaloyes, "Controllable spiking patterns in long-wavelength vertical cavity surface emitting lasers for neuromorphic photonics systems," Appl. Phys. Lett. **107**, 241103 (2015).
15. B. J. Shastri, M. A. Nahmias, A. N. Tait, A. W. Rodriguez, B. Wu, and P. R. Prucnal, "Spike processing with a graphene excitable laser," Sci. Rep. 6, 19126 (2016).
16. P. R. Prucnal, B. J. Shastri, T. Ferreira de Lima, M. A. Nahmias, and A. N. Tait, "Recent progress in semiconductor excitable lasers for photonic spike processing," Adv. Opt. Photonics **8**, 228–299 (2016).
17. P. R. Prucnal and B. J. Shastri, "Neuromorphic Photonics," (CRC, Taylor & Francis Group, 2017).
18. A. N. Tait, M. A. Nahmias, Y. Tian, B. J. Shastri, and P. R. Prucnal, "Photonic neuromorphic signal processing and computing," in "Nanophotonic Information Physics," M. Naruse, ed. (Springer Berlin Heidelberg, 2014), Nano-Optics and Nanophotonics, pp. 183–222.
19. A. L. Hodgkin, and A. F. Huxley, "A quantitative description of membrane current and its application to conduction and excitation in nerve," J. Physiol. **117**, 500–544 (1952).
20. B. Liu, C. Yang, H. Li, Y. Chen, Q. Wu and M. Barnell, "Security of neuromorphic systems: Challenges and solutions," 2016 IEEE International Symposium on Circuits and Systems (ISCAS), Montreal, QC, 2016, pp. 1326–1329.
21. B. Wu, B. J. Shastri, P. Mittal, A. N. Tait., and P. R. Prucnal, "Optical signal processing and stealth transmission for privacy," IEEE J. Sel. Topics Signal Process. **9**, 1185–1194 (2015).
22. L. Xu, B. C. Wang, V. Baby, I. Glesk, and P. R. Prucnal, "All-optical data format conversion between RZ and NRZ based on a Mach-Zehnder interferometric wavelength converter," IEEE Photon. Technol. Lett. **15**, 308–310 (2003).
23. C. G. Lee, Y. J. Kim, C. S. Park, H. J. Lee, and C. S. Park, "Experimental demonstration of 10-Gb/s data format conversions between NRZ and RZ using SOA-loop-mirror," J. Lightwave Technol. **23**, 834–841 (2005).
24. C. H. Kwok, and C. Lin, "Polarization-insensitive all-optical NRZ-to-RZ format conversion by spectral filtering of a cross phase modulation broadened signal spectrum," IEEE J. Sel. Topics. Quantum Electron. **12**, 451–458 (2006).
25. J. Dong, X. Zhang, J. Xu, D. Huang, S. Fu, and P. Shum, "40 Gb/s all-optical NRZ to RZ format conversion using single SOA assisted by optical bandpass filter," Opt. Express **15**, 7587–7593 (2007).
26. A. Tait, M. Nahmias, B. Shastri, and P. R. Prucnal, "Broadcast and weight: An integrated network for scalable photonic spike processing," J. Lightwave Technol. **32**, 3427–3439 (2014).
27. S. Ostojic, "Two types of asynchronous activity in networks of excitatory and inhibitory spiking neurons," Nat. Neurosci. **17**, 594–600 (2014).
28. P. Y. Ma, B. J. Shastri, B. Wu, T. Ferreira de Lima, A. N. Tait, M. A. Nahmias, and P. R. Prucnal, "Spike coded bit sequence generation using photonic excitable laser," in Proc. IEEE Photon. Conf. (IPC), Waikoloa, Hawaii, USA, Oct. 2016, paper MF4.4.
29. B. J. Shastri, M. A. Nahmias, A. N. Tait, B. Wu, and P. R. Prucnal, "SIMPEL: Circuit model for photonic spike processing laser neurons," Opt. Express **23**, 8029–8044 (2015).
30. D. G. H. Nugent, R. G. S. Plumb, M. A. Fisher, and D. A. O. Davies, "Self-pulsations in vertical-cavity surface emitting lasers," Electron. Lett. **31**, 43–44 (1995).
31. S. A. Javro, and S. M. Kang, "Transforming Tucker's linearization laser rate equations to a form that has a single solution regime," J. Lightwave Technol. **13** 1899–1904 (1995).
32. "Synopsys HSPICE," http://www.synopsys.com/tools/Verification/AMSVerification/CircuitSimulation/HSPICE/.
33. M. A. Nahmias, A. N. Tait, B. J. Shastri, T. Ferreira de Lima, and P. R. Prucnal, "Excitable laser processing network node in hybrid silicon: analysis and simulation," Opt. Express **23**, 26800–26813 (2015).

1. Introduction

Spiking is a hybrid information processing technique combining both the bandwidth efficiency of anolog processing and noise robustness of digital computation [1]. It is recognized by the neuroscience community as a sparse coding strategy that widely exists in neural systems [2,3], and has motivated the recent bloom of neuromorphic spike processing primitives in both the electronic domain [4–7] and optical domain [8–15]. Photonic neuromorphic spike processing aims to support both infomation processing and communication on a unified platform [15–17], and promises advantages in efficiency, correctness and adaptability over von Neumann architectures for solving certain tasks such as pattern recognition, decision-making, optimization and learning [17, 18]. Spiking laser exhibiting excitability [19], i.e., excitable lasers, have been viewed as promising candidates of neuromorphic photonic systems through their strong analogy with biological

Optics EXPRESS

neurons [8]. Such an isomorphism has been experimentally demonstrated in a semiconductor microring laser [9], a laser diode driven by a resonant tunneling diode photodetector [10], an optically injected microdisk laser [11], a semiconductor laser with external feedback [12], a micropillar laser in conjunction with a saturable absorber (SA) [13], and vertical cavity surface emitting lasers (VCSELs) [14]. The excitable laser using graphene as the SA, in particular, has been demonstrated to operate at a fast response time on picosecond time scales, and exhibit novel spike processing features such as sharp thresholding and temporal integration [15].

Information is traditionally encoded in the binary format, which is used in widespread digital devices and systems. Nevertheless, it is unclear how spike-based neuromorphic hardware (such as those listed above) will interface with the digital world. For example, the emerging neuromorphic systems have piqued the interest of the research community about their potential cyber-security applications [20], and we recently proposed using excitable lasers for key generation and optical encryption based on the binary data shared by two parties [21]. However, the binary data needs to be first converted to its corresponding spike format before it can be applied to the subsequent neuromorphic spike processing. Conventionally, such a data format conversion can be performed by the widely deployed non-return-to-zero (NRZ) to return-to-zero (RZ) format conversion in fiber-optic communication systems [22–25]. Unfortunately, these NRZ-to-RZ conversion techniques would require (a) many components either implemented on bench or fabricated on chip, and (b) clock signal synchronization which makes them unsuitable for asynchronous operations with spiking neurons [26, 27].

In this paper, we propose and demonstrate a simple and effective interfacing solution that can enable a robust all-optical digital-to-spike (DTS) conversion using a single graphene excitable laser (GEL) without clock signal synchronization. We follow up with our preliminary study of generating the spike coded bit sequence in response to a binary data input modulated in the on-off keying (OOK) format [28]. We perform numerical simulations based on the circuit model of an integrated GEL whose DTS conversion rate can reach 10 Gbps. Our DTS conversion scheme can be operated with flexible OOK input power conditions by adjusting its spike output energy and conversion rate. Moreover, it exhibits a strong capability of restoring the logic-level distorted by the noise via generating spike output with negligible timing jitters. We corroborate the feasibility of our approach with a proof-of-principle experiment using a fiber-based GEL, which achieves a DTS conversion rate of 40 Kbps, and a bit error rate (BER) of 10^{-9} when the OOK input power is −24 dBm.

2. Principle

Here, we summarize the theoretical framework of a two-section excitable laser consisting of a gain section and an SA section, which can be further mapped to an equivalent laser neuron circuit model for numerical calculations [29]. We start with the coupled rate equations describing the carrier concentrations n_χ (subscript $\chi = a$ or s represents either the gain or SA region) and photon number N_{ph} of the gain and SA regions [30]:

$$\frac{dn_\chi}{dt} = \frac{\eta_{i,\chi} i_\chi}{qV_\chi} - \frac{n_\chi}{\tau_\chi} - \Gamma_\chi g(n_\chi)\frac{N_{ph}}{V_\chi} \tag{1}$$

$$\frac{dN_{ph}}{dt} = -\frac{N_{ph}}{\tau_{ph}} + V_a \beta B_r n_a^2 + \Gamma_a g(n_a) N_{ph} + \Gamma_s g(n_s) N_{ph} \tag{2}$$

where $\eta_{i,\chi}$ is the current-injection efficiency, i_χ is the injection current, q is the electron charge, V_χ is the cavity volume, τ_χ is the carrier lifetime, Γ_χ is the optical confinement factor, τ_{ph} is the photon lifetime, β is the spontaneous emission coupling factor, B_r is the bimolecular recombination term. Equation (1) associates the rate of change of the carrier density in the gain and SA regions with the current injection, carrier recombination and stimulated emission. Equation

Optics EXPRESS

Table 1. Parameter list for integrated graphene excitable laser adapted from [29]

Param.	Description	Value
q	Charge of an electron	1.602×10^{-19} C
h	Planck's constant	6.626×10^{-34} J · s
c	Speed of light in vacuum	2.998×10^{8} m · s^{-1}
k	Boltzmann's constant	1.381×10^{-23} J · K^{-1}
T	Temperature of excitable laser	290 K
λ	Lasing wavelength	1575 nm
$\eta_{i,a}$	Current-injection efficiency of gain region	0.70
$\eta_{i,s}$	Current-injection efficiency of SA region	0.70
V_a	Volume of gain region	0.255×10^{-18} m^3
V_s	Volume of SA region	0.085×10^{-18} m^3
Γ_a	Confinement factor of gain region	0.034
Γ_s	Confinement factor of SA region	0.034
τ_a	Carrier lifetime of gain region	100 ps
τ_s	Carrier lifetime of SA region	10 ps
τ_{ph}	Photon lifetime	2.4 ps
η_c	Output power coupling coefficient	0.01
β	Spontaneous emission coupling factor	1×10^{-4}
B_r	Bimolecular emission coupling factor	3×10^{-14} m^3 · s^{-1}
g_a	Differential gain and loss of gain region	0.97×10^{-12} m^3 · s^{-1}
g_s	Differential gain and loss of SA region	14.5×10^{-12} m^3 · s^{-1}
$n_{0,a}$	Transparency carrier density of gain region	1.1×10^{24} m^{-3}
$n_{0,s}$	Transparency carrier density of SA region	1.1×10^{24} m^{-3}
$n_{eq,a}$	Equilibrium carrier density of gain region	7.86×10^{15} m^{-3}
$n_{eq,s}$	Equilibrium carrier density of SA region	7.86×10^{15} m^{-3}

(2) attributes the rate of change of the photon number inside the laser cavity to the photon decay, carrier recombination and stimulated emission. Here, we approximate the carrier-dependent gain to be $g(n_\chi) = g_\chi(n_\chi - n_{0,\chi})$ where g_χ is the differential gain and loss coefficient, and $n_{0,\chi}$ is the optical transparency carrier density [31]. The laser output power P_{out} is related to the number of photons inside the cavity via

$$P_{out} = \frac{N_{ph}\eta_c hc}{\lambda\tau_{ph}} = v_{out}^2 \tag{3}$$

where η_c is the output power coupling coefficient, h is Planck's constant, c is the speed of light in vacuum, λ is the lasing wavelength, and v_{out} is the output voltage used to parameterize P_{out}. We also map the carrier densities within the gain and SA regions to the corresponding bias voltages v_χ across cavity χ through

$$n_\chi = n_{eq,\chi} exp(\frac{qv_\chi}{nkT}) \tag{4}$$

where $n_{eq,\chi}$ is the cavity equilibrium carrier density, $n = 2$ is the typical diode ideality factor for III-V devices, k is Boltzmann's constant, T is the temperature of the excitable laser.

Substituting Eq. (3)-(4) into Eq. (1)-(2) transforms the rate equations into the equivalent laser neuron circuit model recently proposed in [29], which not only captures the underlying photon-carrier interactions within an excitable laser but also simplifies the computation of rate equations for transient analysis purpose. Moreover, this laser neuron circuit model can be fully integrated with the HSPICE circuit simulator provided by Synopsys [32], and offers a direct

Optics EXPRESS

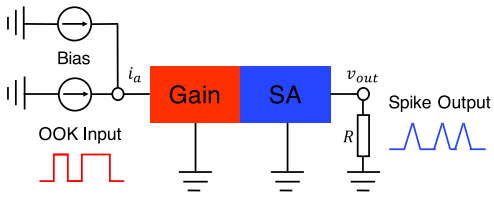

Fig. 1. Simulation setup of the DTS conversion using the integrated GEL.

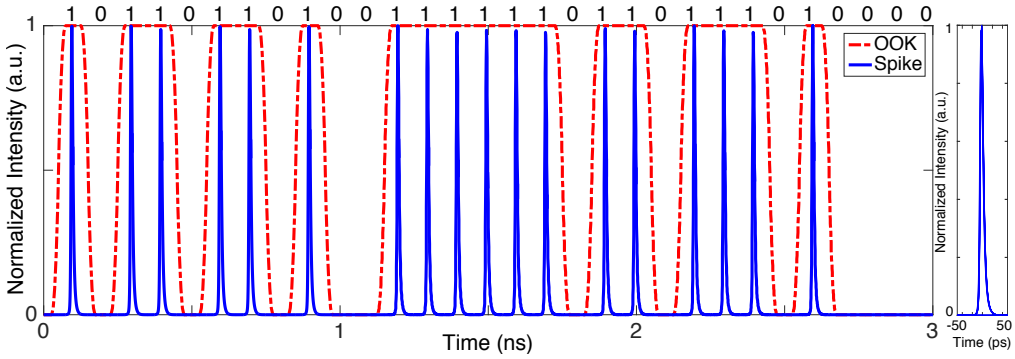

Fig. 2. Left: numerical simulation of the 10 Gbps DTS conversion using the integrated GEL. Right: eye diagram of the spike sequence.

Table 2. Parameter list for the OOK input and corresponding spike output.

Param.	**Value**
OOK input power	27.5 mW
OOK input bit period	100 ps
Spike output FWHM	7.12 ps
Spike output peak power	1.5 mW
Spike output interval	100 ps
Spike output generation rate	10 Gbps

relationship between the output voltage v_{out} and injection current i_χ. Our simulations focus on an integrated GEL (e.g., the one proposed in [33] and [15]), which contains an electrically pumped gain medium and graphene sheets as the SA. We provide realistic material and geometrical parameters of the integrated GEL in Table 1.

3. Numerical simulation

We study the DTS conversion mechanism of an integrated GEL via numerical simulations. Figure 1 shows the circuit simulation setup that drives the GEL circuit model. To operate the two-section laser in the excitable regime, its gain section is biased just below the laser threshold, i.e., with a bias current of 16 mA in this case. There is no bias current to the SA section. We provide the OOK input as an external injection current to the gain section, which adopts a $2^{10}-1$ pseudo-random bit sequence (PRBS). Note than excitable lasers can be perturbed either electrically after O/E conversion (as in the hybrid platform [33]) or optically. Examples of optically injected excitable lasers include an integrated two-section micropillar laser [13], and polarization switching VCSELs [14]. Here, we model the input as an injection current because we use the circuit model to characterize the carrier and photon dynamics of the excitable laser with a circuit simulator. The bias current and OOK input together constitute the injection current

Optics EXPRESS

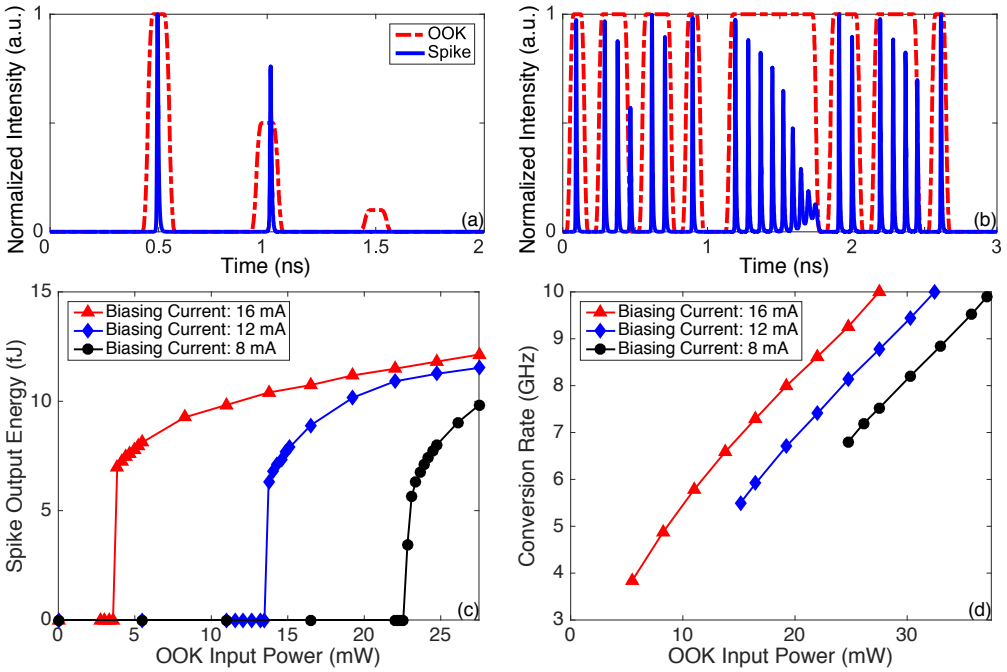

Fig. 3. (a) Illustration of the spike output versus OOK input power variations. The OOK input power are 27.5 mW (left), to 13.75 mW (middle), and to 2.75 mW (right), respectively. (b) The DTS conversion when the OOK input power is 30.25 mW. (c) The spike output energy versus the OOK input power at various biasing conditions. (d) The DTS conversion rate versus the OOK input power at various biasing conditions.

to the gain section i_a. The spike output is represented as the voltage output v_{out} at the edge of the SA section whose measurement is enabled by a dummy load R (with a large resistance).

The GEL generates the spike sequence corresponding to the digital bit pattern. For every bit, the gain carrier concentration is temporally perturbed (continuously integrated) by the input energy before reaching an excitable threshold (determined by the bias). Meanwhile, the SA saturates, releasing the accumulated photon energy in the form of a spike, and depleting the gain. As the gain carrier concentration recovers to equilibrium, the GEL experiences a refractory period, during which time the arrival of another excitatory input cannot trigger the release of another spike. Usually, the refractory period is lower bounded by the carrier lifetime of the gain and SA sections together [15]. Here, the refractory period, and thus the output spike interval, is determined by the slower of the two carrier lifetimes of the gain (i.e., 100 ps) and SA (i.e., 10 ps). Consequently, the upper limit of the GEL's DTS conversion rate in the present case is 10 Gbps. The waveforms in Fig. 2 (left) show such a DTS conversion, and the corresponding waveform parameters are listed in Table 2. We also plot the eye diagram [Fig. 2 (right)] of the spike sequence where the spike output traces overlap each other, verifying that the integrated GEL relies on no clock signal for synchronization purpose. This is especially significant for reducing the system complexity and implementation cost of a network of integrated GELs, which can be operated on asynchronous inputs without the necessity of providing each input with a local clock signal.

Next, we examine the DTS conversion of the integrated GEL as a function of the OOK input power. The OOK input bit period is set to be 100 ps while the bias current remains at 16 mA. On one hand, Fig. 3(a) shows three single-bit DTS conversions when we reduce the OOK input power from 27.5 mW (left), to 13.75 mW (middle), and to 2.75 mW (right). Less spike output energy is

Optics EXPRESS

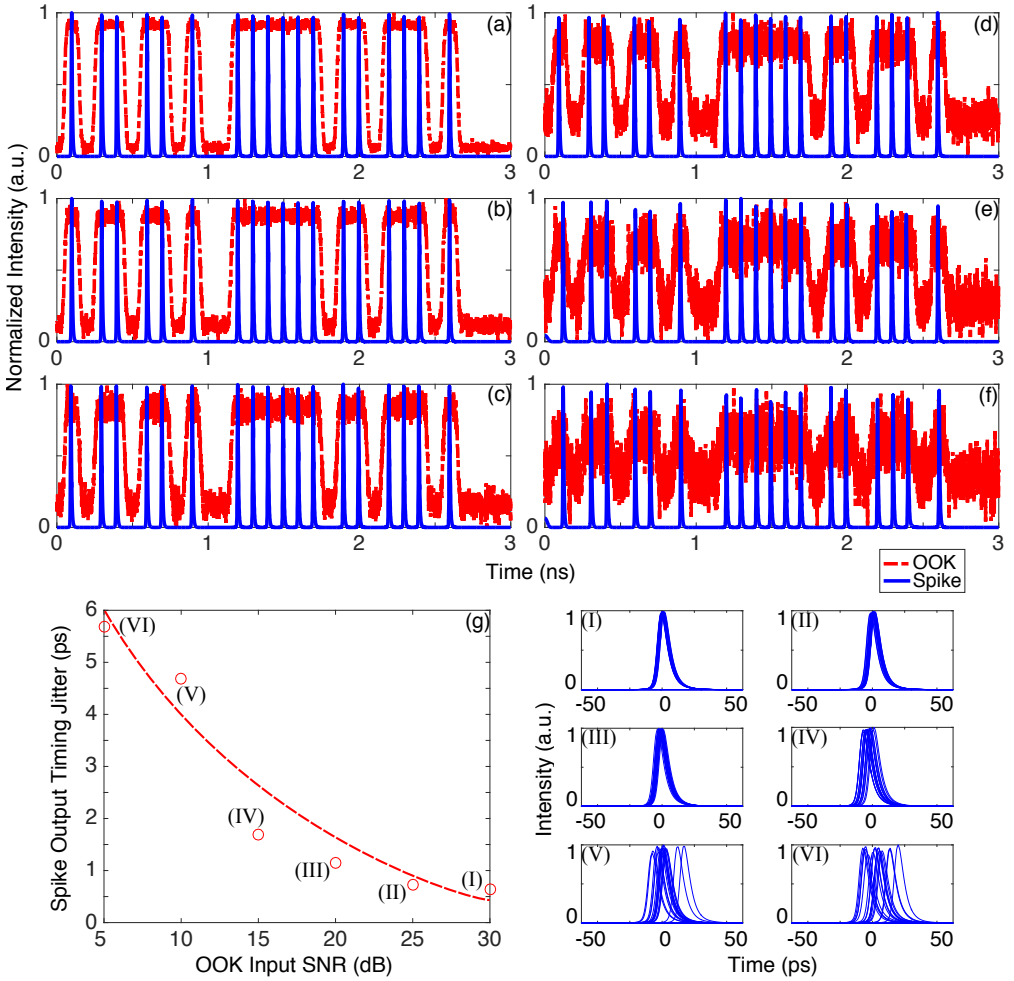

Fig. 4. Numerical simulation of the DTS conversion using the integrated GEL when the OOK input has an (a) SNR = 30 dB, (b) SNR = 25 dB, (c) SNR = 20 dB, (d) SNR = 15 dB, (e) SNR = 10 dB, (f) SNR = 5 dB. (g) Left: timing jitter of the spike output with respect to the OOK input SNR. Right: corresponding eye diagrams (I–VI).

obtained in subject to lower OOK input power, and the spike output is completely suppressed when the OOK input cannot bring the gain carrier concentration above the excitable threshold. On the other hand, the GEL is unable to carry out the DTS conversion faithfully when we increase the OOK input power to 30.25 mW [as shown in Fig. 3(b)]. This is because the conversion rate in this case is upper bounded at 10 Gbps such that any further increase in the OOK input power will not bring about any increase in the conversion rate, but disrupt the excitable dynamics within the GEL instead.

In Fig. 3(c) and 3(d), we illustrate respectively the spike output energy and the DTS conversion rate versus the OOK input power at various biasing conditions. Here, based on the spike output peak power P_{out} [Eq. (3)] and its full width at half maximum (FWHM) τ_{FWHM}, we calculate the spike output energy as $P_e = P_{out} \times \tau_{FWHM}/0.88$. Given the same OOK input power in Fig. 3(c), the spike output energy is larger at a high biasing current than that at a low biasing current. It can also be concluded that the higher the biasing current, the lower the excitable threshold. In Fig. 3(d), such a thresholding position is found to affect the conversion rate range, which is

Optics EXPRESS

upper bounded at 10 Gbps for all biasing conditions. For a biasing current of 16 mA, the GEL may perform DTS conversion at 3.85 Gbps even if the OOK input power is lowered to 5.5 mW. However, the GEL can only operate at 6.8 Gbps or above with a biasing current of 8 mA. The wide range of the DTS conversion rate at a given biasing condition offers the flexibility that shall benefit future neuromorphic photonic systems where GELs may process information at various operation speeds.

Signal noise can limit the application potential of data conversion systems. Here, we study the noise tolerance and jitter generation of the GEL. We add white Gaussian noise to the previous 10 Gbps OOK input to perform DTS conversion at multiple OOK input signal-to-noise ratios (SNRs) and show the corresponding waveforms in Fig. 4. As we increase the amount of noise added to the OOK input from SNR = 30 dB [Fig. 4(a)] to SNR = 5 dB [Fig. 4(f)], the OOK input logic-level is gradually distorted to the point where we can hardly identify the bit period from the OOK input. The integrated GEL, however, demonstrates a surprisingly strong tolerance of the noise by still managing to generate the *same* spike sequence regardless of the amount of noise added to the OOK input.

Figure 4(g) further shows the relationship between the timing jitter of the spike output and the OOK input SNR. The timing jitter of individual spike output refers to the timing deviation of the spike output from its ideal position within each bit period (i.e., the spike output position without noise addition in Fig. 2). The timing jitter for a given OOK input SNR is calculated by the standard deviation of the timing jitters among all the output spikes. We notice a clear increasing tendency of the timing jitter as we move from high SNR to low SNR. An ultra-low timing jitter of 645 fs is achieved at SNR = 30 dB, while the timing jitter is 5.68 ps for SNR = 5 dB which is only about 5% of the total 100 ps bit period. We also show the eye diagrams [Fig. 4 (right)] of the spike sequence at different OOK input SNR, which validates this tendency with less overlapping among spike output samples as we increase the amount of noise added to the OOK input. The spike output timing jitter results from the fact that the OOK input noise disrupts the energy accumulation rate inside the integrated GEL so that the average energy accumulation rate does not remain the same for each bit. However, the overall OOK input noise influence is not noticeable unless there is a considerable amount of noise. Even at low OOK input SNRs (e.g., at SNR = 5 dB), our DTS conversion approach may still successfully restore the OOK input logic-level that has been severely distorted by the noise. Such noise robustness and its associated small timing jitter further demonstrate that our technique not only requires no clock signal synchronization, but also generates the spike sequence that could potentially serve as an excellent clock recovery source from which the clock information can be extracted.

4. Experimental demonstration

As proof-of-principle, we demonstrate the DTS conversion mechanism using a benchtop fiber-based excitable laser [15] (Fig. 5). The two-section ring cavity consists of a 75-cm long highly-doped erbium-doped fiber (EDF) as the gain medium, and a film of chemically synthesized graphene (sandwiched between two fiber connectors) as the saturable absorber. The gain and SA sections are separated by an isolator (ISO) to ensure unidirectional propagation and a polarization controller (PC) to enhance spike output stability. The EDF is pumped by a 980 nm laser diode through a 980/1550 nm wavelength division multiplexer (WDM). An arbitrary waveform generator (Agilent 33220A) modulates a 1480 nm laser diode to generate a digital PRBS input which is coupled into the laser with a 1480/1550 nm WDM. Note, the PRBS pattern is the same as that in numerical simulations (Sec. 3). The spike signal at 1550 nm is decoupled out of the system through the 20% port of the 20/80 coupler.

We present a clip of the OOK input and spike output in Fig. 6 containing the same 30 bits as that in Fig. 2. The waveform parameters are detailed in Table 3. For the OOK input, the bit period is set to be 25 μs and the bit rate is 40 Kbps. No clock signal is needed for synchronization

Optics EXPRESS

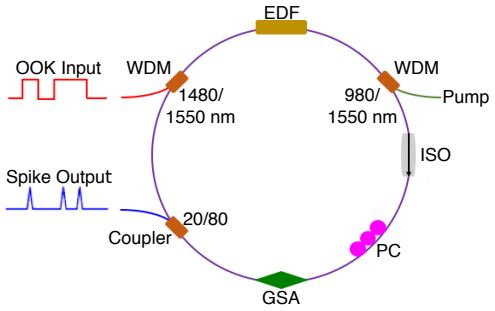

Fig. 5. Experimental setup of the DTS conversion using the fiber-based GEL.

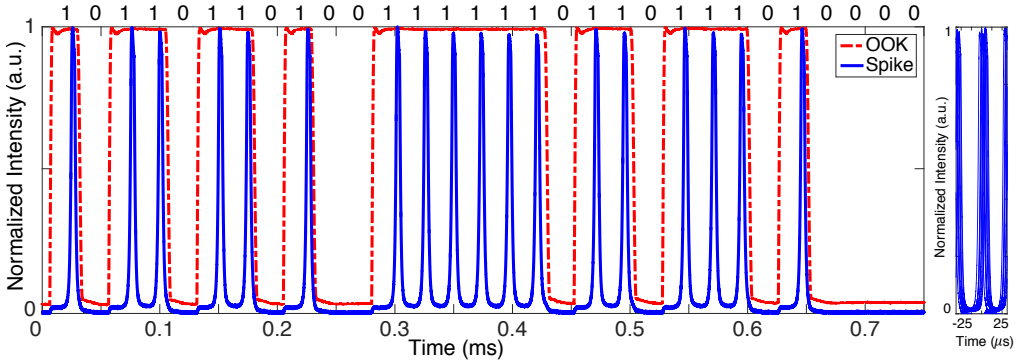

Fig. 6. Left: experimental demonstration of the DTS conversion using the fiber-based GEL. Right: eye diagram of the spike sequence.

Table 3. Parameter list for the OOK input and corresponding spike output. (* mean values of the parameters)

Param.	**Value***
OOK input power	−24 dBm
OOK input bit period	25 μs
Spike output FWHM	3.92 μs
Spike output peak power	−23.66 dBm
Spike output interval	24.8 μs
Spike output generation rate	40 Kbps

purpose (as validated by the eye diagram of the spike sequence shown on the right side). The consecutive spike output interval is measured to be 24.8 μs, which corresponds to a limited DTS conversion rate of approximately 40 Kbps. The much slower rate of the fiber-based prototype compared to that of the integrated GEL is due to the facts that: 1) the gain region volume of the fiber-based prototype ($\sim$ cm^3) is much larger than that of the integrated GEL ($\sim$ μm^3); and 2) the carrier lifetime of the fiber-based prototype ($\sim$ ms) is much longer than that of the integrated GEL ($\sim$ ns). It is worth mentioning that there has been no report on the fabricated integrated GEL so far, and this is the very first experimental demonstration of the DTS conversion using the GEL.

Figure 7 shows the DTS conversion accuracy as the measured BER versus the OOK input power. Here, we maintain the same bit rate for the OOK input but change its power. We start from the OOK input power of −24 dBm which is also the power condition under which the above waveforms are obtained, and attenuate the OOK input power all the way down to −29 dBm.

Optics EXPRESS

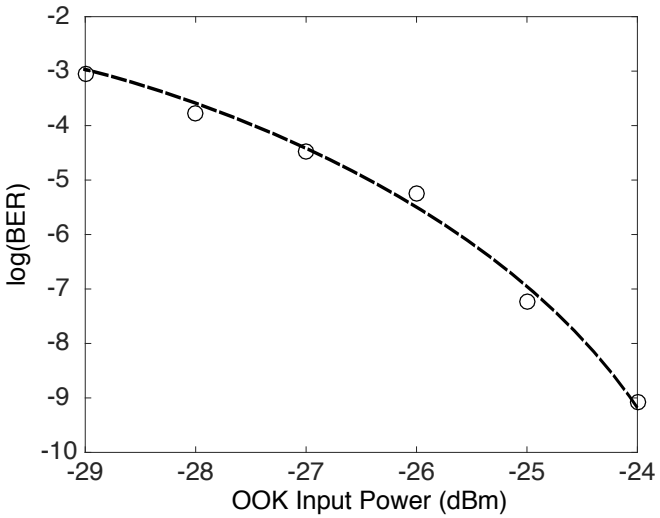

Fig. 7. BER measurement of the DTS conversion using the fiber-based GEL.

During this process, the BER degrades from 10^{-9} to 10^{-3}, which is due to the reduction of the OOK input power that causes the GEL to take longer time to respond with one spike output for one incoming bit 1 of the OOK input. Hence, the BER results mainly from missing the last spike of a long sequence of consecutive bit 1s.

5. Conclusion

In this paper, we propose using a single GEL to convert the binary data in the OOK format to its spike counterpart without clock signal synchronization. The numerical simulation based on an integrated GEL exhibits a DTS conversion rate up to 10 Gbps. Our scheme provides flexible operation modes at various OOK input power conditions, and robust logic-level restoration under strong noise interference. The proof-of-principle experiment using the fiber-based GEL verifies the feasibility of our approach by operating at a relatively lower speed and achieving a 10^{-9} BER with an OOK input power of −24 dBm. Our technology could potentially assist the neuromorphic spike processing in interfacing with the binary operation system. Future work will involve empirical demonstration of the DTS conversion using the on-chip integrated GEL. Cavity volumes and carrier lifetimes of the gain and SA sections of the laser limit the conversion rate. Further increase in the conversion rate can be achieved by reducing the volumes or lowering the carrier lifetimes (e.g., via proton bombardment techniques to create defect states) of the gain and SA sections.

Funding

National Science Foundation (NSF) Award (EECS 1642962).